

SELECTED PROBLEMS AND SOLUTIONS IN THE DESIGN
 OF THE SLAC 40-INCH HYDROGEN BUBBLE CHAMBER

J. Ballam, R. Blumberg, J. Mark, K. Skarpaas, S. St. Lorant
 Stanford Linear Accelerator Center, Stanford, California

A 40-inch-diameter by 20-inch-deep hydrogen bubble chamber is being constructed at the Stanford Linear Accelerator Center with scheduled operation by July 1967. The purpose of this contribution is to describe some special design features which have already been tested. The general properties of the chamber are given in Table I. The size was chosen as being the largest consistent with a two and one-half year construction schedule to give a chamber useful for 4-8 GeV physics. This energy range was determined from analysis of monochromatic photon beams obtainable from $e^+ e^-$ annihilation in flight as analyzed by Ballam and Guiragossian,¹ and by Chadwick,² as well as a FAKE³ program analysis adapted for this purpose by W. B. Johnson of SLAC which showed that four-constraint events were thoroughly analyzable up to 8 GeV and one-constraint events up to 6 GeV at magnetic fields of 22 kG. It is well recognized that this chamber would probably be inadequate for precision work at energies greater than 10 GeV.

TABLE I
 Features of the SLAC 40-Inch Hydrogen Bubble Chamber

Visible volume of LH ₂	400 liters
Nominal diameter	40 inches
Depth	20 inches
Thickness of vertical front glass	7.7 inches
Expansion system	Bellows-sealed piston (hydraulically driven with a repetition rate of 2 per sec)
Beam Window	≈1/8-inch-thick beryllium
Magnetic Field	22 kilogauss (3 megawatts)
Magnet Weight	250 tons of iron and 35 tons of copper
Refrigeration system	Bulk liquid hydrogen
Illumination system	Scotchlite
Film format	70 mm sprocketed - 3 views on one strip

The special features to be described are:

- I. The toroidal, hydroformed expansion bellows.
- II. The piston design and the hydraulic expansion system.
- III. The magnetic steel backplate and other special materials used in construction of the chamber.

Other general features are briefly described below.

1. Beam Window. A $28\text{-}1/8 \times 6\text{-}1/8 \times 1/8$ -inch beryllium beam window (0.57 gm/cm^2) is mounted in the chamber itself. There will also be a beam window of $1/4$ -inch-thick aluminum in the vacuum tank, 22 feet upstream of the chamber. A magnet will sweep away charged particles made in this window. From a safety point of view, the beryllium window is treated as if it were made of glass.

2. Magnet Transport. The magnet will have no special transport system. Gross lateral motion will be accomplished with rollers. Motor driven jacks will provide the vertical motion. At SLAC beam height (7 feet), an eight-inch downward motion is allowed, while a large upward motion can be achieved with cribbing. Lateral adjustments up to one foot will be possible with auxiliary jacks. A separation system using lead screws will split the magnet up to distances of 10 feet.

3. Portability. The chamber, magnet and building are designed so that the complete assembly can be relocated in another beam in one to two months time.

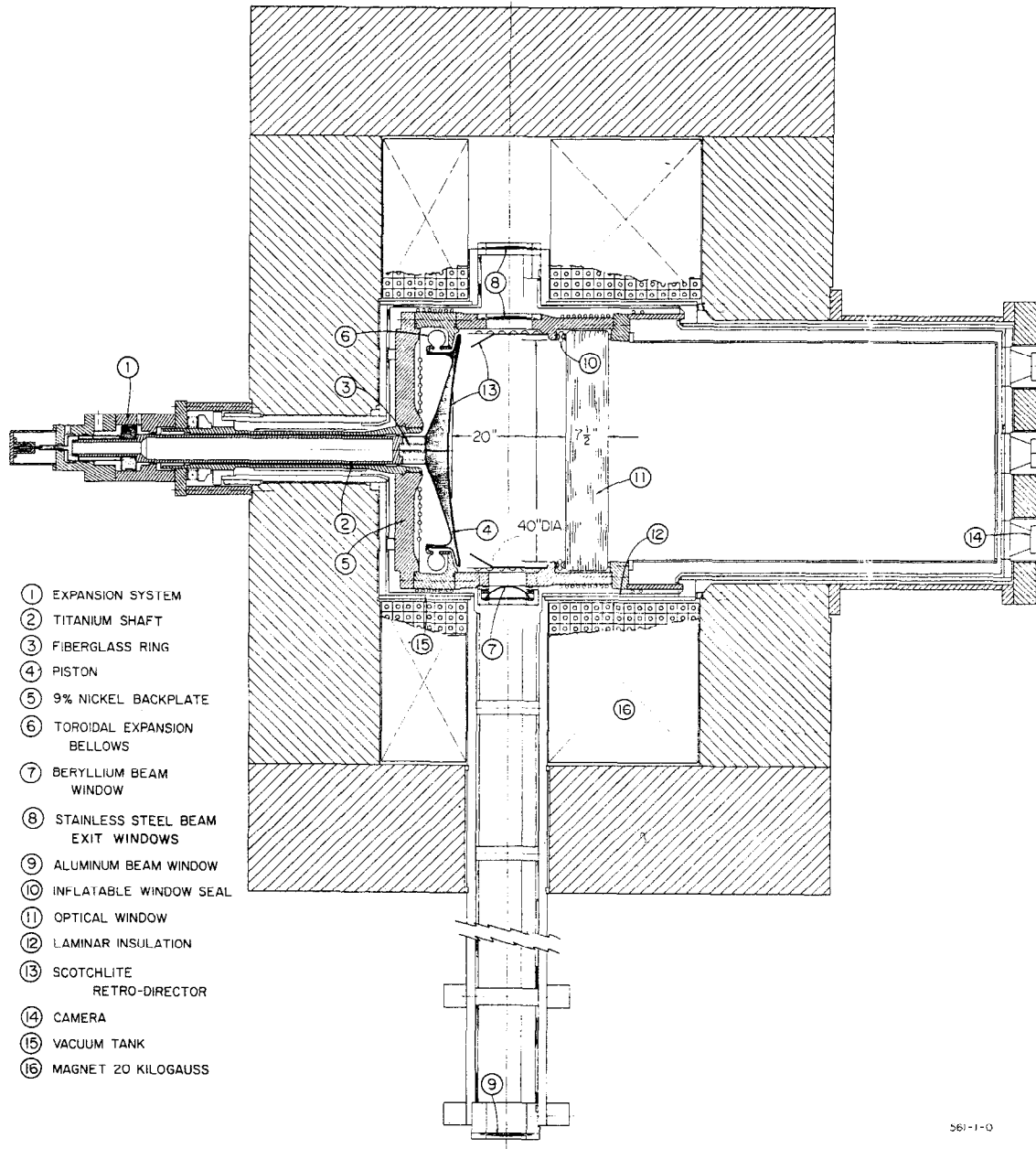
A cross section of the chamber is shown in Fig. 1.

I. THE EXPANSION BELLOWS FOR THE 40-INCH HYDROGEN BUBBLE CHAMBER

A. Introduction

The cross section of the toroidal expansion bellows for the bubble chamber is shown in Fig. 2. Such "omega" bellows have the property that alternating stresses are a minimum and pressure stresses are almost independent of the major diameter. A right-circular toroidal convolution is similar in behavior to a circle of thin tubing, in which the stresses at any pressure are a function of the minor radius and of the wall thickness. As the torus is hydraulically formed, it is free from circumferential welds, which could act as local stress concentrators. The toroidal convolution is formed about heavy, integral reinforcing bands in such a manner that only the concave part of the torus is subject to flexure.

The stress calculation is based on the solution of the inhomogeneous differential equations determining rotationally-symmetric stress distributions in thin elastic shells of revolution. The method of dealing with the coupled, second-order equations most suited for this purpose has been given by Clark and Reissner⁴ and by Clark^{5, 6} in the asymptotic approximation of $\mu > 1$ where $\mu = \sqrt{12(1 - \nu^2)} \frac{b^2}{ah}$. Here ν is Poisson's ratio for the material in question, a is the major radius of the torus taken between centers, b is the minor radius of the cross section, and h is the thickness of the shell. In the present case where $a = 20$ inches, $b \approx 1.5$ inches, $h \approx 0.030$ inch, and $\nu = 0.305$, $\mu = 12.38$, so that the approximation is sufficiently good. Experience shows that an accuracy to within 5 to 10 percent of the measured stresses⁷ can be achieved with the method, without recourse to elaborate computer calculations. If λ defines the parameter b/a (≈ 0.075 in this case) then, in general, the relative accuracy of the formulae used is determined by the order at which the expansion is stopped, usually $\sim \lambda/\mu^{1/3} \approx 3.2 \times 10^{-2}$.



361-1-0

FIG. 1--Horizontal cross section of the SLAC 40-inch bubble chamber.

B. Stresses Due to Motion of Bellows

It is assumed that the behavior of the shell due to a vertical deflection of the edge of the gap may be approximated by considering separately the action of the top and bottom halves of the torus. Thus, in the top half of the omega joint the tangents to the meridian remain vertical at the outer and inner edges. These edges are not subject to radial shear. Within the approximation of $\mu > 1$, the most significant stresses are then the circumferential direct stress σ_D and the meridional bending stress σ_B .

According to the solution of Ref. (5), the maximum hoop stress occurs very near the crown line, while the maximum meridional bending stress occurs at points on either side of the crown line.

The method of solution given in Ref. (6) then leads to two expansions of the type.

$$\sigma_{D, \max} = \alpha \left(\frac{h}{b^2} \right)^{1/3} - \beta \left(\frac{h}{b^2} \right) \quad (1)$$

$$\sigma_{B, \max} = \pm \gamma \left(\frac{h}{b^2} \right)^{1/3} \pm \eta \left(\frac{h}{b^2} \right) \quad (2)$$

where

$$\alpha = \frac{0.0987 E \delta}{(1 - \nu^2)^{1/6} a^{2/3}} = 4.770 \times 10^4$$

$$\beta = \frac{0.0987 E \delta}{(1 - \nu^2)^{1/2}} \times \frac{0.342}{12^{1/3}} = 5.42 \times 10^4$$

$$\gamma = \frac{0.1371 E \delta}{(1 - \nu^2)^{2/3} a^{2/3}} = 6.950 \times 10^4$$

$$\eta = \frac{0.1371 E \delta 0.054}{(1 - \nu^2) \times 12^{1/3}} = 1.250 \times 10^4$$

C. Stresses Due to Internal Pressure

Since the edges of the torus are effectively restrained from moving radially, the stresses due to internal pressure are assumed to be the same as those existing in a complete toroidal shell subjected to a pressure in a like manner. The stresses are obtained from an elementary consideration of equilibrium in thin shells:

$$\sigma_D = \frac{1}{2} \left(\frac{bp}{h} \right); \quad \sigma_B = \left(\frac{2a + b}{a + b} \right) \quad (3)$$

where p is the internal pressure.

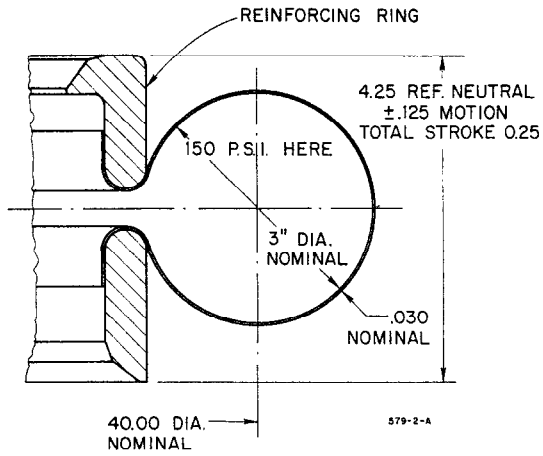


FIG. 2--Cross section of omega expansion bellows.

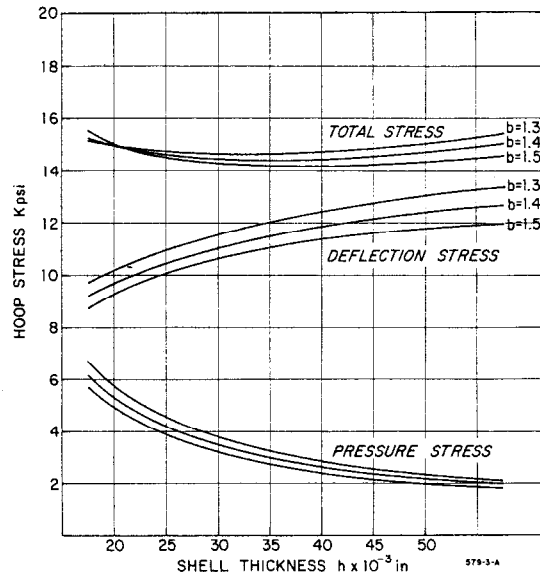


FIG. 3--Hoop stresses in bellows as a function of shell thickness.

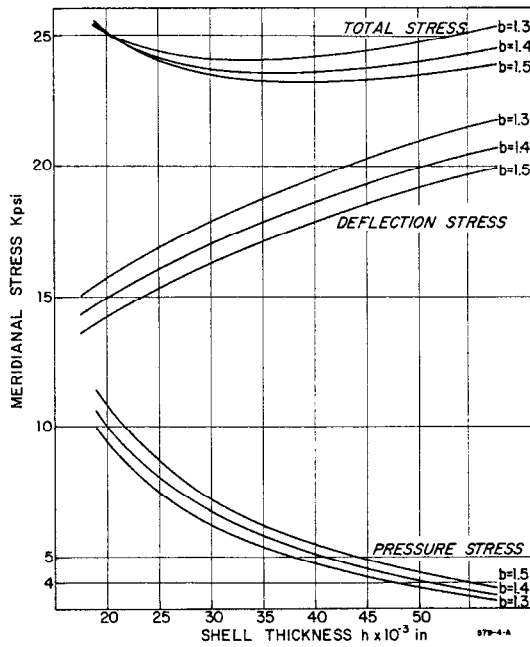


FIG. 4--Meridional stresses in bellows as a function of shell thickness.

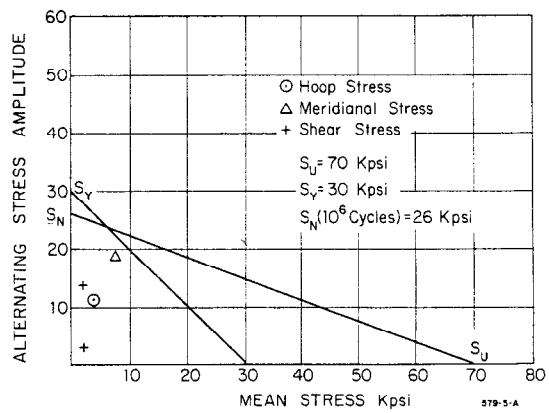


FIG. 5--Goodman fatigue diagram.

D. Design of the Bellows

The following parameters were used to calculate b and h.

Material

ASME type SA240 - 316L stainless steel

Modulus: 28.0×10^6 psi

Poisson's ratio: 0.305

Operating Conditions

Pressure: Dynamic : 150 psig
 Static : 225 psig

Temperature: 20° C

Excursion: (2δ) 0.250 inches

Bellows Construction

Major radius: 20 inches

Minor radius: Not to exceed 1.6 inches

The maximum stresses in the bellows are given by the algebraic sums of Eqs. (1), (2), and (3). The two resulting relations have stationary (minimum) points when b and h reach their optimum values, but note that it is not possible to minimize σ_D and σ_B simultaneously at these points.

In the present case, the value of b is imposed by the design of the bubble chamber so that values of h can be obtained from these relations. For example, with b = 1.5 inch, $h \approx 0.030$ inch for minimum hoop stresses and $h \approx 0.037$ inch for minimum bending stresses.

The variation of the principal stresses as a function of b and h over a range of values is shown in Figs. 3 and 4. It is concluded that a toroidal expansion bellows with a = 20 inches, b = 1.5 inches, and h = 0.031 inches would satisfy the design criteria.

E. Fatigue Analysis

The calculated maximum, mean, and amplitude variations of the principal stresses are presented in Table II and the result of a conventional Goodman diagram-type of analysis shown in Fig. 5. A distortion energy calculation leads essentially to the same results.

TABLE II

	<u>Maximum Stress</u>		<u>Mean Stress</u>	<u>Ampl. of Variable Stress</u>	
	Expansion S_e	Compression S_c	S_m	S_{alt}	$S_{equiv.}$
Hoop Stress	+14300	- 6800	3800	10600	11200
Outer	- 9000	+23500	7200	16300	18200
Meridional Stress					
Inner	+23500	- 9000	7200	16300	18200
Outer	-11700	+15200	1700	13400	13800
Shear Stress					
Inner	+ 4600	- 1100	1700	2900	2900

Note: $S_{equiv.} = \left(S_{alt} \right) / \left(1 - (S_m / S_u) \right)$

For the analysis, the strain-cycling fatigue data prescribed by Section III of the ASME Boiler and Pressure Vessel Code were adopted. These curves show the allowable amplitude of the alternating stress component (one-half of the alternating stress range) plotted against the number of cycles. The fatigue curves average the uniaxial strain-cycling data of all 18 - 8 stainless steels below 800° F. From the curves it would appear that at 20° C a bellows fatigue life in excess of 10^6 cycles can be expected.

At the temperature of liquid hydrogen a similar fatigue curve⁸ would indicate a bellows fatigue life of the order of 5×10^7 cycles.

F. Bellows Test

The bellows were specified as shown in Fig. 2, but the four units received deviated somewhat from this shape. The gap and hence the overall height of the bellows varied from 0.7 to 1.0 inches and the minor cross-section departed from circularity by as much as 0.6 inches in the worst case.

In the pressure, vacuum, and life tests, the bellows were compressed to the design height. Two bellows at a time were tested in opposition at a cycling rate of 4 to 6 cycles per second. See Fig. 6.

The first set of two bellows was cycled $\approx 10^6$ times at room temperature with 150 psig pressure in the bellows without failure. The second set of two bellows was cycled 10^5 times under identical conditions while strain measurements were made.

Two sets of five paper-base strain gauges of different gauge lengths and resistance, but identical in response to cyclic loading, were distributed in the regions of the expected maximum stresses. A typical set of values for the meridional stress is shown in Table III. The error in the measurements was ± 3 percent.

TABLE III

Condition of Test	Measured Stress (psi)	Calculated Stress (psi)
No pressure in bellows	19,000	16,500
150 psig in bellows: fast cycling frequency (8 cps)	21,700	23,400
150 psig in bellows: low cycling frequency (1/2 cps)	21,000	23,400

As the bellows were mounted in the test fixture in a pre-stressed state, before the strain gauges were applied, the stresses measured represent the alternating forces produced by the motion of the bellows, superimposed on the steady bias of the deformation force.

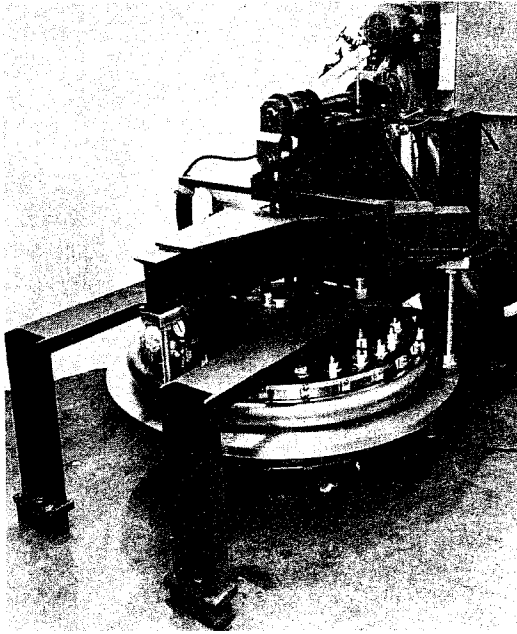


FIG. 6--Expansion bellows test fixture.

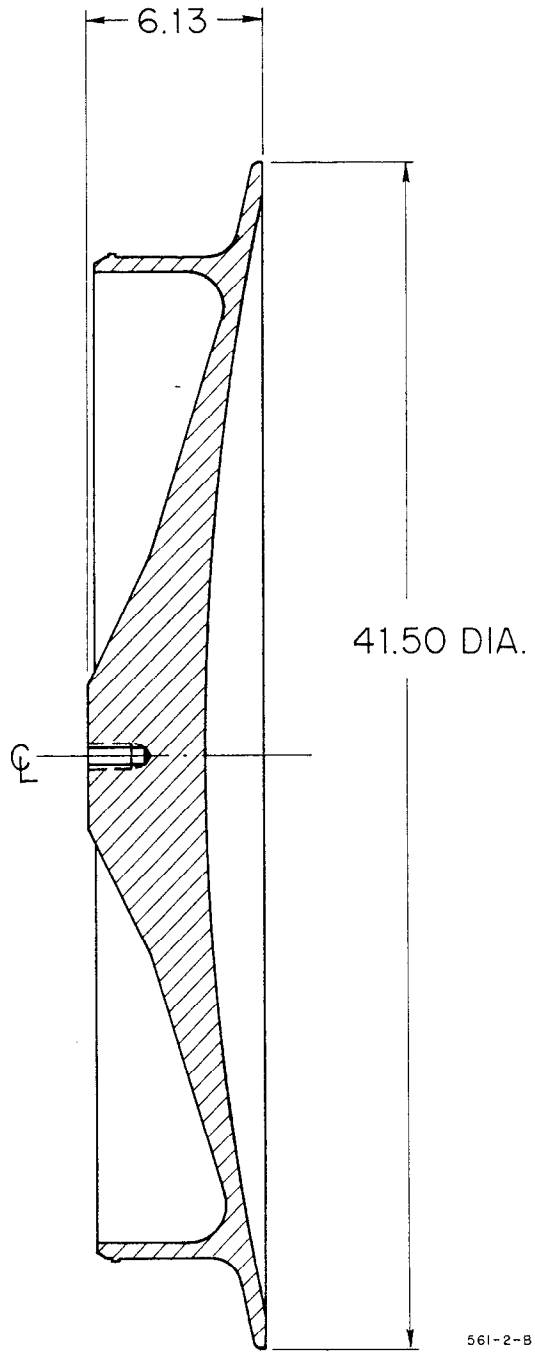


FIG. 7--Cross section of expansion piston.

The spring constant of one bellows with a 3/4-inch gap was measured by uniformly loading the bellows until the gap was reduced to 3/8 inch. The experimental value of 5000 lb./in. was in good agreement with the predicted value.

II. PISTON DESIGN AND THE HYDRAULIC EXPANSION SYSTEM

Eddy current heating of the piston as it moves in the slightly inhomogeneous magnetic field could be reduced by using a non-conducting material, for example epoxy-glass combinations. However, as the technology of such materials requires further development, the stainless steel alloy Kromarc 55 was selected for the piston material as it was used for the chamber body and its mechanical properties have been carefully evaluated. Because stainless steel has an appreciable electrical conductivity, the piston weight was minimized. Also, the low mass simplified the expansion system.

The piston is shown in Fig. 7 and resembles a large automotive type poppet valve. The spherical shape of the inner surface allows the change-over from Scotchlite to a mirror should this turn out to be necessary.

A. Calculation

The approximations to the required thickness were made using several flat plate stress formulae. Approximation 1 assumed a circular plate of varying thickness with radial slots to eliminate hoop stresses. Approximation 2 (Ref. 9) assumed that the reaction force was uniform over a 4-inch circle in the center of the back of the plate. The load was a pressure of 150 psi. The thickness was then calculated as a function of the radius while maintaining a constant radial stress of 20,000 psi. Approximation 3 increased the area of the reaction circle to that radius for which the thickness was calculated. Approximations 2 and 3 were then repeated while maintaining a constant hoop stress of 20,000 psi. None of the flat plate approximations were accurate because of the dished contour of variable thickness. The shape chosen was heavier than that required by the radial stress formulae while in some places it was not as thick as indicated by the hoop stress considerations.

B. Tests

The piston was machined and 28 strain gauges were bonded to the back surface. The piston was then held in a fixture to duplicate the chamber edge conditions and subjected to compressive load and hydraulic pressure in the 600,000-lb. compression testing machine installed at the U. S. Naval Post Graduate School, Monterey, California. The radial and hoop stresses at maximum test load are summarized in Table IV. Out to a radius of 13.5 inches, the piston is reasonably close to a constant stress plate, but for larger radii, the stresses are lower, probably due to the strengthening effect of the attachment ring. The piston stresses under operating conditions will be about one-half of these test conditions. Inertia loading under normal operation or malfunction is expected to be the equivalent of 30 psi when the snubber decelerates the piston at 30 G. The piston was tested for pressure loading without axial load to simulate conditions during repair to the hydraulic system. It was also tested with an axial load but no pressure load to simulate loading caused by a malfunction of the hydraulic system. No permanent deformations were caused by the testing.

TABLE IV
Expansion Piston Stresses at 150 psi

Radius (Inches)	Radial Stress Measured	Hoop Stress Measured	Flat Plate Approximation Hoop Stress
3.0	9,600	16,000	14,300
4.5	12,200	13,500	16,300
6.0	11,300	19,100	19,100
7.5	8,400	26,900	25,900
9.0	13,800	25,500	30,400
10.5	10,400	24,000	↑ Not applicable ↓
12.0	No gauge	25,600 est.	
13.5	2,800	18,400	
15.0	- 4,800	7,300	
Rim	- 7,200	4,900	
18.0	No gauge	12,800 est.	
19.5	No gauge	13,400 est.	

C. Expansion System

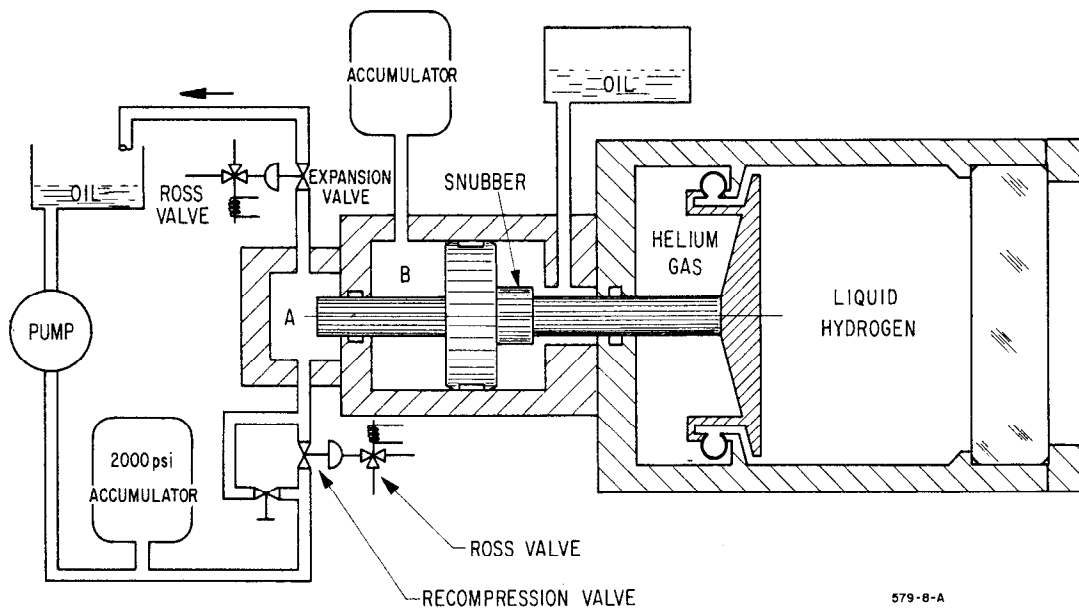
The expansion system is shown schematically in Fig. 8. The force of the liquid hydrogen is normally balanced by the sum of the hydraulic pressures acting on the small pistons A and B, which are 4-3/8 inches and 8 inches in diameter, respectively.

The attempt was made to use a resonant system so that the expansion energy is stored in an accumulator and is used in helping the recompression. The resonant system was designed in analogy with a simple spring, with its equilibrium or "balance" point being the piston position at half its maximum stroke.

This "balance" principle is analogous to suspending a weight from a spring. The point where it hangs freely is the "balance point." If the weight is lifted 1/8 inch the bubble chamber is compressed. Suddenly releasing the force holding the weight up will allow the weight to oscillate $\pm 1/8$ inch about the "balance point" until some force stops it. In the case of the hydraulic system, damping assumes this function. A hydraulic snubbing system is built in to limit the maximum stroke in case pressures are not set correctly, or if the chamber is filled with gas and does not act like a spring. Every stroke is supposed to end with the piston resting against a mechanical stop. The approach to that stop is snubbed hydraulically by trapping some oil behind piston B. A manual valve controls the cushioning effect.

The key to the success of this resonant system lies in the fast operating, large volume flow hydraulic expansion and recompression valves. These were designed and built at SLAC. A drawing of one of the valves is shown in Fig. 9. These valves open or close in 5 milliseconds and pass up to 150 gal/min of oil.

The valves are pneumatically piloted. They are held closed by air pressure on top of the 3-inch piston C. The air pressure needs to be just a little more than 1/9 of the oil pressure on the bottom port. In this system,



579-8-A

FIG. 8--Schematic of expansion system.

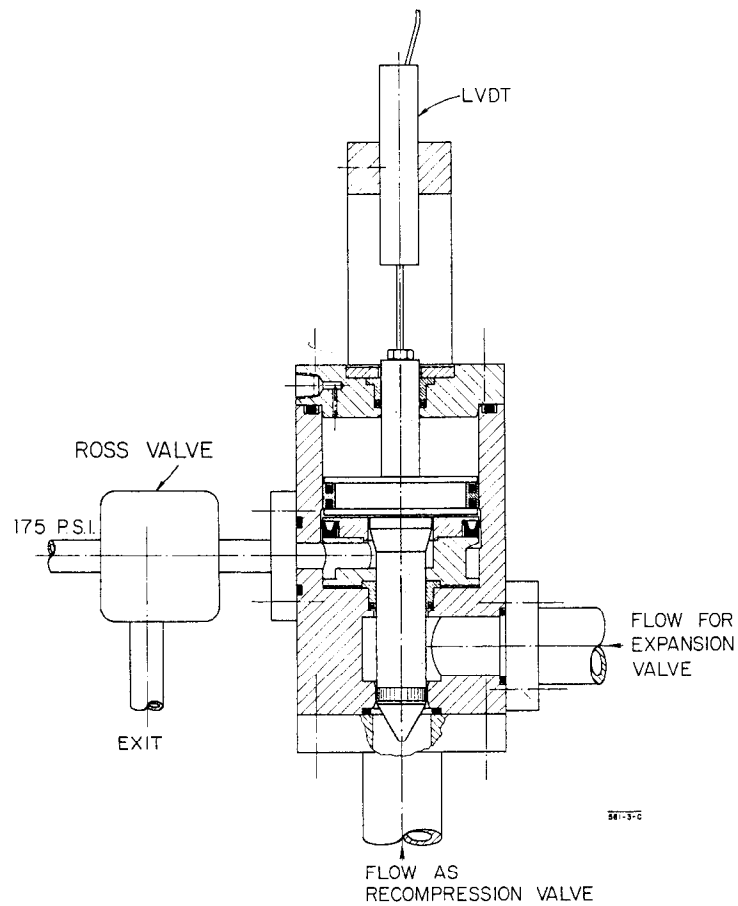


FIG. 9--Cross section of expansion valve.

the pulsing pressure of the piston A connects to the side port of the valve. The low pressure sump connects to the bottom port of the expansion valve. The high pressure supply connects to the bottom of the recompression valve. This arrangement requires air pressure of about 225 psi to balance the force of the oil at 3000 psi. Ross 3-way pneumatic valves are used to pilot the fast hydraulic valves. The Ross valves are modified to take a linear variable differential transformer (LVDT) to monitor the movement of their poppets. Similar LVDT's also monitor the hydraulic valves and the main piston displacements. With this instrumentation, a change in operating characteristics can be diagnosed and corrected very quickly.

A hydraulic bubble chamber simulator was built to test the system. It consists of a 10-inch piston the same weight as the chamber piston, and acting against oil pressure 16 times the chamber pressure. The system was proof tested to 10^6 cycles. It was found necessary to use seals made of 90 durometer polyurethane. No failures of the seals took place during the testing. A photograph of the apparatus is shown in Fig. 10.

It is interesting to note that a 5-horsepower hydraulic unit pumping 2 gallons per minute at 3000 psi or 2.9 gallons per minute at 2300 psi is used. About 5 c.f.m. of air at 200 psi are needed to pilot the valves. The air compressor also requires almost 5 horsepower for 2 pulses per second. During the testing which sometimes approached 3 pulses per second, the 10 horsepower compressor unit in use has a 50 percent duty cycle. Compared with non-resonant expansion systems for chambers of this size, the power expenditures are small.

A typical displacement-time curve obtained from these tests is shown in Fig. 11. Expansion and recompression each take about 12-1/2 milliseconds. The braking of the return stroke is clearly seen.

III. MAGNETIC STEEL BACK PLATE

In order to increase the magnetic field and improve its uniformity, a back plate of steel, which remained magnetic at low temperatures, was required. Low carbon, 9 percent nickel steel was developed commercially to meet the need for a material of moderate cost with good welding and forming qualities that would be satisfactory for service at temperatures down to that of liquid nitrogen. This material has been tested extensively down to the temperature of liquid nitrogen,¹⁰ and it is now produced as plates and forgings according to ASTM designations A-352 and A-522, respectively.

To guarantee the integrity and the superior mechanical properties at liquid hydrogen temperature, forgings were produced from steels which were electric furnace air-melted and vacuum degassed. Forging soundness was further ensured through rigid ultrasonic inspection. The two forgings were produced by Lenape Forge,¹¹ a division of Bonney Forge Incorporated.

The testing of the mechanical properties was performed by an independent testing laboratory¹² and the following results were obtained:

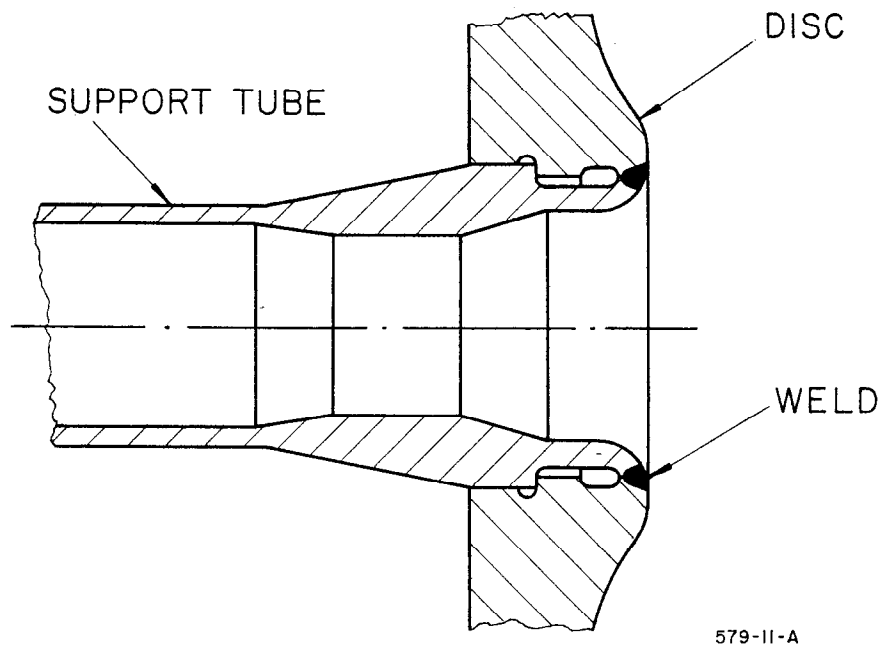


FIG. 10--Cross section of weld.

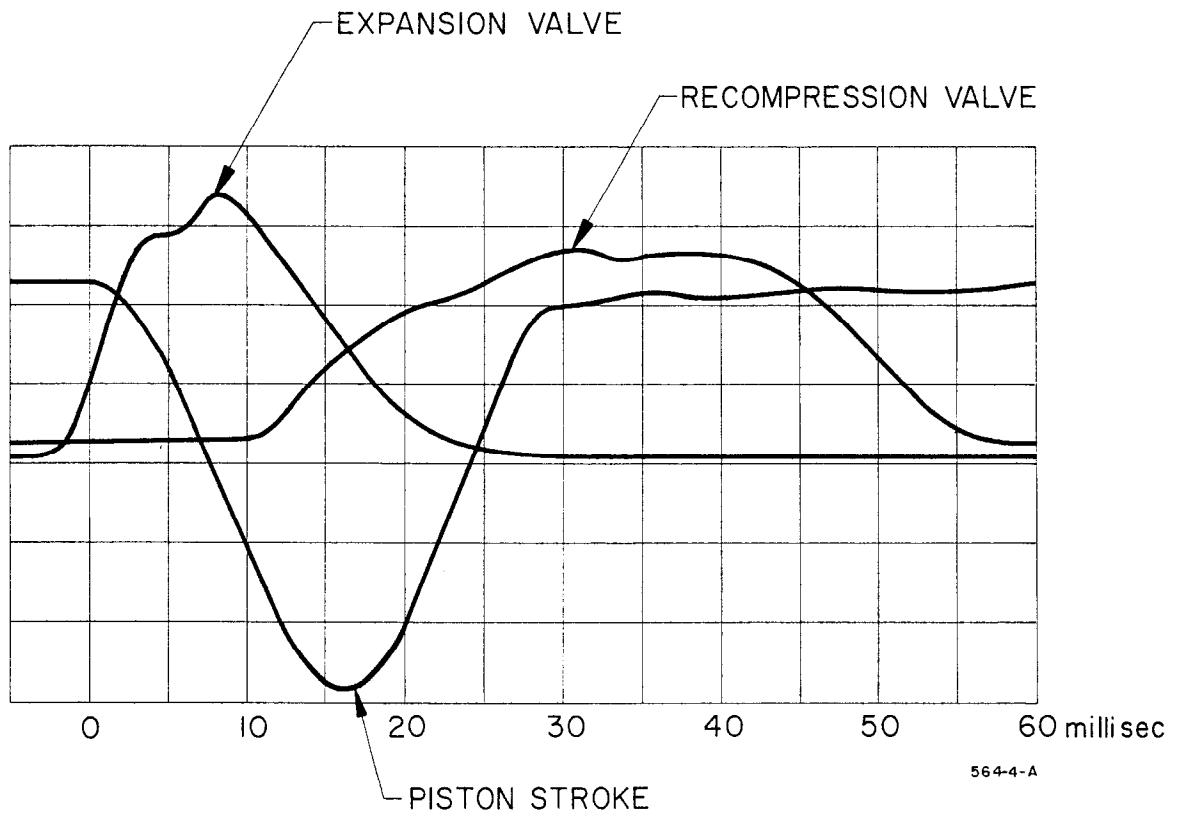


FIG. 11--Displacement-time curves for the hydraulic bubble chamber simulator.

TABLE V

	First Disk	Second Disk	Tube
Tensile stress (psi)	92,000	103,400	105,200
Yield stress (psi)	82,500	82,500	94,600
Elongation in % in 2-inches	9.0	28.0	23.0
Reduction of area (%)	15.6	74.0	54.8
Charpy V-Notch Impact Valve in ft. lb. at -320° F	Avg. 59	56	84
Charpy V-Notch Impact Valve in ft. lb. at -400° F	46	55	73
Ultrasonic tests	Rejected because of internal flaking	Accepted	Accepted

The welding was performed at SLAC, Fig. 11, using the Tungsten Inert Gas Welding process with pure argon as shielding gas. The filler was 1/16-inch-diameter Inco-Weld A wire. Several test welds were made which provided the same amount of restraint on the weld deposit as the final weld. From these were determined the amount of peening and the corresponding interpass temperature which gave the least strained finished assembly.

The 9-percent nickel steel weldment will during certain conditions in this installation be exposed to loads which produce maximum compressive stresses of 30,000 psi and maximum tensile stresses of 22,000 psi.

The magnetic properties of 9-percent nickel steel at room and cryogenic temperatures were investigated by H. Brechna.¹³ He compared the hysteresis loop and saturation of 9-percent nickel steel with 0.1-percent low carbon ARMCO ingot steel in dc magnets at different temperatures. He found that the saturation value at 300° K of 9-percent Ni-Fe is 20,815 gauss, or 4.52 percent lower than low carbon steel (21,800 gauss); at 78° K (liquid N₂ temperature) the saturation value is 20,834 gauss, and at 4.2° K it is 21.9 gauss. The deviation of the saturation values for 9-percent Ni-Fe from room temperature to 4.2° K is 0.89 percent, and from 300° K to 78° K about 0.1 percent.

Acknowledgements

The authors wish to express their thanks to the staff of the bubble chamber group for their assistance in the project.

References

1. J. Ballam and Z. Guiragossian, Intern. Conf. on Instrumentation in High Energy Physics, Dubna, 1964 (to be published).
2. J. Ballam, G. Chadwick, Z. Guiragossian, D. Leith, W. Johnson and R. Larsen, SLAC Experimental Proposal 8, Appendix I, Stanford Linear Accelerator Center, Stanford, California.
3. G. R. Lynch, UCLRL - 10335, Lawrence Radiation Laboratory, Berkeley California (July 1962).

4. R. A. Clark and E. Reissner, Adv. Appl. Mech. II, 93 (Academic Press, 1951).
5. R. A. Clark, J. Math. and Phys. 29, 146 (1950).
6. R. A. Clark, Quart. of Appl. Mach. 16, 47 (1958).
7. N. C. Dahl, A.S.M.E. Trans 75, 497 (1953).
8. Cryogenic Materials Data Handbook, AD618 065 (July 1965).
9. R. J. Roark, Formulas for Stress and Strain, Third Edition, p. 199 (1954); Case No. 11.
10. The International Nickel Company.
11. Lenape Forge, P.O. Box 536, Westchester, Pa., 19380.
12. Lehigh Testing Laboratory, Wilmington 99, Delaware.
13. H. Brechna, SLAC Internal Report 65-87, Stanford Linear Accelerator Center, Stanford, California (1965).